Modeling the turbulent heat fluxes in low Prandtl number shear flows

T. Baumann[1], A. Loges[1], L. Marocco[2], T. Schenkel[1,3], T. Wetzel[1] and R. Stieglitz[1]
[1] Karlsruhe Institute of Technology (KIT), Karlsruhe, Germany
[2] Politecnico di Milano, Milano, Italy
[3] FAU Busan, Friedrich-Alexander-Universität Erlangen-Nürnberg - Busan Campus, Republic of Korea
t.baumann@kit.edu, andre.loges@kit.edu, luca.marocco@polimi.it,
torsten.schenkel@busan.fau.de, thomas.wetzel@kit.edu, robert.stieglitz@kit.edu

Abstract

Liquid metals are often considered for an effective convective heat transport in several technical applications. Since the geometric setup is in most cases quite complex, and additionally the Reynolds numbers are large, numerical simulations frequently use a Reynolds-averaged Navier-Stokes equations (RANS) approach. Hereby, the turbulent heat fluxes are applied inadequately by a constant turbulent Prandtl number Pr_t. In this context, different advanced Pr_t models are compared and analyzed with experimental and Direct Numerical Simulation (DNS) data, which are conceived as validated. The different simulations show an improvement of the thermal field, but also depict the influence of the eddy viscosity model for forced and mixed convective flow.

1. Introduction

Heavy liquid metals (HLM) are considered as coolant and target material in the concept of accelerator driven systems (ADS) for the transmutation of radioactive waste. The heat generated in the fuel assembly must be reliably transferred to the primary cooling liquid at any operational condition taking advantage of the relative high specific thermal conductivity of the liquid metal. The geometric complexity and high Reynolds numbers presuppose the RANS approach to represent turbulence in numerical simulations in the majority of technical applications. For safety reasons a reliable description of the turbulent heat fluxes and therefore, a validation of the introduced models is mandatory. Modeling them by introducing Pr_t as constant can result in a significant inaccuracy related to the transferred heat. Furthermore, turbulent flows of low Prandtl number liquids exhibit different wall normal extensions and spectral behavior of both, the turbulent heat flux and Reynolds stress distribution. A more sophisticated modeling is required regarding these quantities. This demands a profound knowledge on the heat transfer and turbulence characteristics near the wall determining the technical performance of the most crucial components.

In this paper different methods for improved modeling of the turbulent heat fluxes are analyzed, and the results of RANS simulations are compared with DNS and with experimental data for higher Reynolds numbers. A validation of the velocity profile, the temperature profile, the turbulent viscosity and Pr_t of different shear flows is carried out. Therefore, a simplified experiment was built up in the Karlsruhe Liquid Metal Laboratory (KALLA) to study a single

heated rod which is concentrically embedded in a pipe and cooled by Lead-Bismuth eutectic (LBE). The challenges of turbulence modeling are elaborated for fully developed shear flow problems such as the channel flow or the concentric annulus, and are transferred to the forced and mixed convective flow of the heated rod experiment. Especially the latter is of crucial importance, since it decisively judges about the performance and safety of the reactor at abnormal conditions like a LOFA (loss of flow accident).

2. Basic equations

The Reynolds equations, using the Boussinesq assumption for incompressible flows with buoyancy forces caused by density changes, is given by eq. (1). Here, the density ρ is treated as constant, however buoyancy is considered by introducing a force term expressed by the volumetric expansion [1]:

$$\rho \frac{D\overline{u_i}}{Dt} = -\frac{\partial \overline{p}}{\partial x_i} + \rho \frac{\partial}{\partial x_j}\left(\nu \frac{\partial \overline{u}_i}{\partial x_j}\right) + \beta \rho g_i \left(\overline{T} - T_{ref}\right) - \rho \frac{\partial}{\partial x_k}\overline{u_i' u_k'}. \tag{1}$$

The averaged energy equation using the RANS approach for incompressible flows reads to:

$$\frac{D\overline{T}}{Dt} = \frac{\partial}{\partial x_j}\left(\alpha \frac{\partial \overline{T}}{\partial x_j}\right) - \frac{\partial}{\partial x_k}\overline{u_k' T'}. \tag{2}$$

The equations are written, using the Einstein notation, with the thermal heat conductivity α, the kinematic viscosity ν, the pressure p, the temperature T, the velocity u_i, the directional gravitation constant g_i and the volumetric expansion coefficient β. There are different ways to model the Reynolds stresses R_{ij} in the momentum equations and the turbulent heat fluxes in the energy equation. The simplest way for modeling R_{ij}, called the Boussinesq approach, is introducing a turbulent viscosity ν_t analogous to ν as:

$$R_{ij} = -\overline{u_i' u_j'} = \nu_t \left(S_{ij}\right) - \frac{2}{3} k \delta_{ij} + C_{ext} a_{ij} k. \tag{3}$$

The anisotropy tensor $a_{ij}\left(S_{ij}, W_{ij}\right)$, only considered in nonlinear turbulence models, depends on the strain-rate tensor S_{ij} and the vorticity tensor W_{ij}:

$$S_{ij} = \frac{1}{2}\left(\frac{\partial \overline{u}_i}{\partial x_j} + \frac{\partial \overline{u}_j}{\partial x_i}\right) \text{ and } W_{ij} = \frac{1}{2}\left(\frac{\partial \overline{u}_i}{\partial x_j} - \frac{\partial \overline{u}_j}{\partial x_i}\right). \tag{4}$$

For linear models the nonlinear term is zero $(C_{ext} = 0)$ [2]. Nonlinear and linear viscosity models mostly use the equations for the turbulent kinetic energy k and for its dissipation ϵ as given by eqs. (5) and (6).

$$\frac{Dk}{Dt} = \frac{\partial}{\partial x_j}\left[\left(\nu + \frac{\nu_t}{\sigma_k}\right)\frac{\partial k}{\partial x_j}\right] + P_k + P_B - \epsilon + D, \tag{5}$$

$$\frac{D\epsilon}{Dt} = \frac{\partial}{\partial x_j}\left[\left(\nu + \frac{\nu_t}{\sigma_\epsilon}\right)\frac{\partial \epsilon}{\partial x_j}\right] + C_{\epsilon 1} f_1 \left(P_k + P_B\right) - C_{\epsilon 2} f_2 \frac{\epsilon^2}{k} + E, \tag{6}$$

with the production terms of the turbulent kinetic energy caused by the velocity field and by the thermal field for flows incorporating buoyancy:

$$P_k = -\overline{u_i' u_j'}\frac{\partial \overline{u}_i}{\partial x_j} \text{ and } P_B = -\beta g_j \overline{u_i' T'}. \tag{7}$$

The turbulent viscosity ν_t is a turbulent exchange coefficient of the momentum and is generally modeled by

$$\nu_t = f_\mu C_\mu \frac{k^2}{\epsilon}. \tag{8}$$

The Launder and Sharma (LS) and Lam and Bremhorst (LM) model consider the turbulence isotrope. Both show good agreement for shear flows of low and high Reynolds numbers and describe near-wall flows satisfactory [3]. Both are chosen as momentum turbulence model. Low Reynolds eddy viscosity turbulence models differ only in the choice of different damping functions, source terms, constants and boundary conditions of the two equations as described in [3]. An algebraic approach for the turbulent heat fluxes can be written with some assumptions according to Younis et. al. [4]. For linear eddy viscosity models, we can define the turbulent Prandtl number Pr_t as the ratio of the turbulent viscosity to turbulent thermal diffusivity analogous to the molecular Prandtl number Pr, we get:

$$Pr_t = \frac{\nu_t}{\alpha_t}. \tag{9}$$

In contrast to the molecular one it is a modeling approach. DNS and experiments have shown that applying Pr_t as constant results in unacceptable high inaccuracy for low molecular Prandtl number liquids. Different correlations are available for fully developed shear flows. The simplified Navier-Stokes equation in main flow direction is:

$$0 = -\frac{\partial \overline{p}}{\partial x_1} + \rho \frac{\partial}{\partial x_2}\left(\nu \frac{\partial \overline{u}_1}{\partial x_2}\right) - \rho \frac{\partial}{\partial x_2}\overline{u_1' u_2'}. \tag{10}$$

For shear flows with linear turbulence modeling the simplified characteristic equation for the Reynolds stress normal to the mainstream direction is $-\overline{u_1' u_2'} = \nu_t(\partial \overline{u}_1/\partial x_2)$ and the turbulent heat flux is $-\overline{u_2' T'} = \alpha_t(\partial \overline{T}/\partial x_2)$ with the coordinate system given in figure 1.

2.1 Correlations to model the turbulent Prandtl number *Pr$_t$*

The correlations were all developed for forced convection, linear viscosity turbulence models and shear flows. One approach used in this work is the correlation developed by Cebeci [5]:

$$Pr_t = \frac{\kappa}{\kappa_h} \cdot \frac{1-exp(-y/A)}{1-exp(-y/B)} \approx \frac{\kappa}{\kappa_h} \cdot \frac{1-exp(-y^+/A^+)}{1-exp(-y/B)} \tag{11}$$

$$B = \frac{B^+ \nu}{y_\tau},\ B^+ = \frac{1}{Pr^{0.5}} \cdot \sum_{i=1}^{5} C_{Ci} \left(log_{10} Pr\right)^{i-1},\ A^+ = 26,\ \kappa = 0.4,\ \kappa_h = 0.47$$

$$C_{C1} = 34.96,\ C_{C2} = 28.79,\ C_{C3} = 33.95,\ C_{C4} = 6.300,\ C_{C5} = -1.186. \tag{12}$$

The dimensionless wall distance is defined as: $y^+ = y u_\tau/\nu$ with the shear velocity $u_\tau = \tau_w/\rho$, applying the wall shear stress τ_w. The implicit model by Lin [6], determining the inverse effective eddy Prandtl number γ, is deduced by Renormalization group analysis and yields:

$$\left(\frac{\gamma+2}{1/Pr+2}\right)^{1/3}\left(\frac{\gamma-1}{1/Pr-1}\right)^{2/3} = \frac{1}{1+\nu_t/\nu} \text{ with } \gamma = \frac{1}{Pr}\frac{1+\alpha_t/\alpha}{1+\nu_t/\nu}. \tag{13}$$

The ratios of the turbulent to molecular thermal diffusivity α_t/α and the turbulent to molecular viscous diffusivity ν/ν_t are applied in this correlation. Kays introduced a simple equation for the logarithmic region of the wall layer. It fits the curves of the Yakhot correlation and the exact Pr_t profiles determined from DNS evaluation [7]:

$$Pr_t = \frac{0.7\nu}{\nu_t Pr} + 0.85. \tag{14}$$

The Notter and Sleicher correlation was applied in the notation scheme of Churchill [8] and for linear eddy viscosity models:

$$Pr_t = (1+\phi)\left(\frac{0.025 Pr \frac{\nu_t}{\nu}}{1-\frac{\nu_t}{\nu}} - \phi\right)\left(1 + \frac{10}{35+\frac{\nu_t}{\nu}/\left(1-\frac{\nu}{\nu_t}\right)}\right) \tag{15}$$

$$\text{with} \quad \phi = 90 Pr^{1.5}\left(\frac{\frac{\nu_t}{\nu}}{1-\frac{\nu_t}{\nu}}\right)^{0.25}. \tag{16}$$

3. Validation concept

The validation cases are simulations of a fully developed channel flow with a wall normal constant heat flux as denoted in figure 1 and a fully developed flow in a concentric annulus as depicted in figure 7. Both are validated with DNS from Abe et. al. [9] and Chung et. al. [10]. Finally, the individual approaches are compared to a developing flow along a heated rod in a concentric cavity for which experimental data exists [11]. A general comment to this approach is that coupling of Pr_t to the turbulent viscous dissipation only has some implications.
This approach allows to tackle if correctly done mainly forced and to some extend mixed convective flows. A computation of buoyancy dominated flows is not possible, since the turbulent heat fluxes are inherently coupled to the viscous turbulent dissipation, which assumes that they are proportionally coupled. The approach is better than the conventional ones but nevertheless is of approximate nature. A deficit which can not be overcome by this approach is the entirely different spectral behavior of the temperature field and the velocity field. This would demand an approach as in the TMBF-model [12]. Being aware of the incompleteness of the introduced model assumptions, these advanced models allow a more realistic description at still a fast simulation time. Hence, an additional aspect is to elaborate the reliable limits of the used approach.

3.1 Fully developed channel flow

The fully developed channel flow (figure 1) is a typical validation case for turbulent viscosity models. The momentum field can be validated using the velocity profile and a turbulent value like the turbulent kinetic energy k, the turbulent viscosity ν_t or the turbulent shear stress $\overline{u_1' u_2'}$ to represent the turbulent characteristics. The velocity profiles are made dimensionless by introducing the dimensionless velocity $u^+ = \overline{u}/u_\tau$ and the dimensionless distance $y^+ = y u_\tau/\nu$.

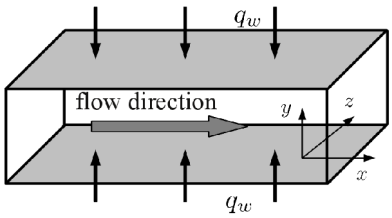

Figure 1: Schematic diagram of the turbulent fully developed channel flow

The turbulence models are validated using data from DNS [9] with two different Reynolds numbers ($Re = 14000$ and $Re = 24000$). The dimensionless velocity profiles (figure 2) show good agreement for both turbulence models in comparison with the averaged dimensionless velocities from the DNS for both Reynolds numbers, especially in the viscous sublayer ($y^+ < 5$) and the transition to wall turbulence layer ($5 < y^+ < 30$). LB determines in contrast to LS a difference of the slope within the logarithmic turbulence layer. ν_t (figure 3) is negligible in the viscous sublayer for both models and the DNS data. The RANS exhibit higher ν_t in the transition layer in contrast the DNS results. The $\nu_{t,LS}$ values are too high and the ones of the LB are too low in the logarithmic layer. It is obvious that the imprecision of the modeled ν_t affects the modeled turbulent heat fluxes by definition of Pr_t.

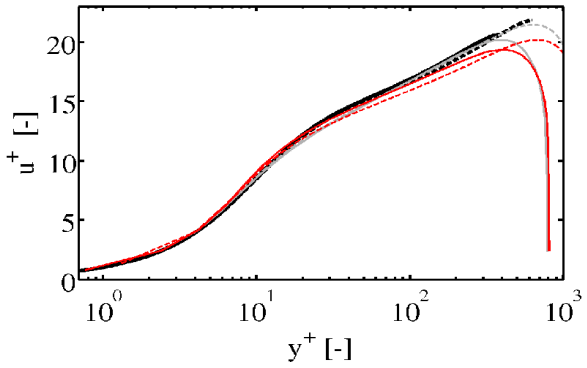

Figure 2: Comparison of the dimensionless velocity profiles for the channel flow as a function of y^+ for different Reynolds numbers

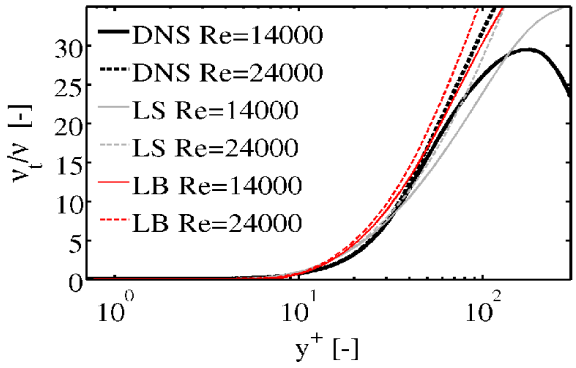

Figure 3: Comparison of the turbulent viscosity for the channel flow as a function of y^+ for different Reynolds numbers

DNS data [13] with a constant normal wall heat flux as boundary condition are analyzed, and the exact Pr_t is compared with the different correlations for $Pr = 0.025$ for the two different Reynolds numbers (figure 4) described in section 2.1. The temperature is treated as a passive scalar. Comparing the correlations with the exact Pr_t, we see differences especially at low y^+ values. But due to the low Pr, the thermal sublayer is stretched more up to $y^+ \approx 50$. Hence, the turbulent heat fluxes are negligible in this part. This can also be shown analyzing the exact α_t profiles in relation to the molecular one (figure 5). Modeling Pr_t as constant, mostly $Pr_t = 0.9$, results in a too high total thermal diffusivity. The modeled α_t is considerably influenced by the modeled ν_t, thus by the turbulence model. There is a high thermal inaccuracy caused by the turbulence model and mainly by using Pr_t as a constant.

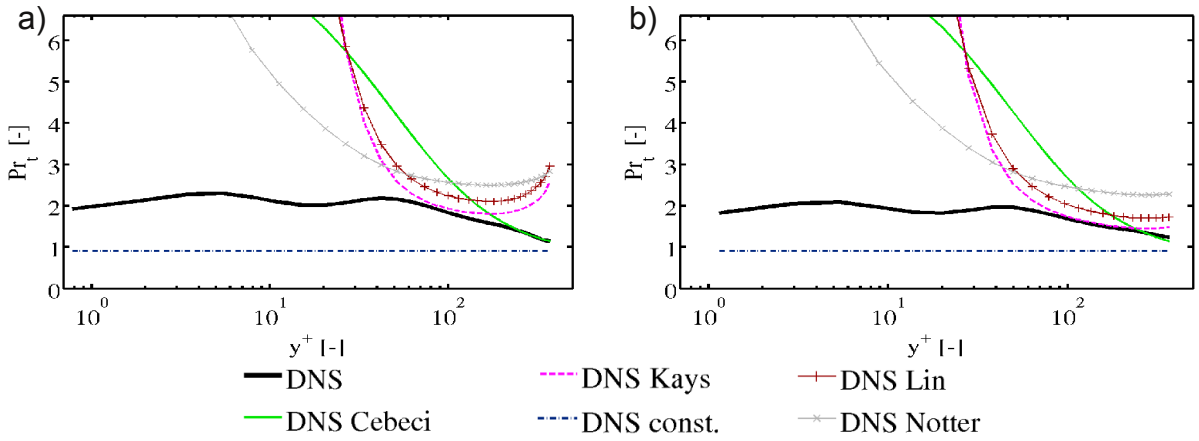

Figure 4: Pr_t determined by different correlations analyzing DNS data as a function of y^+ for different Reynolds numbers, a) *Re = 14000* and b) *Re = 24000*

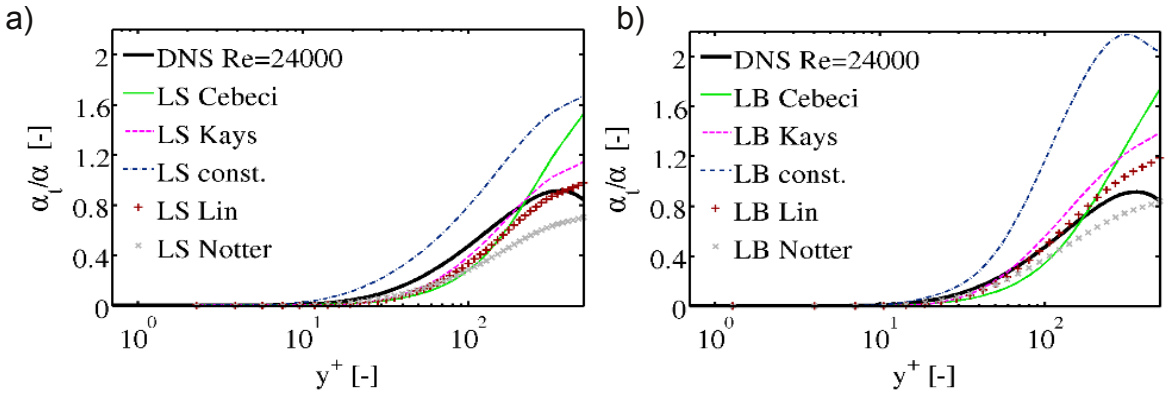

Figure 5: Comparison of exact and modeled turbulent heat diffusivity using different correlations of the Pr_t as a function of y^+ for different turbulence models

In the following, the different Pr_t correlations to model the turbulent heat fluxes are analyzed. a_t shows generally a much better agreement with the DNS in the transition and the logarithmic layer compared with a constant Pr_t. The correlations were all developed for the logarithmic layer. But because of the widened thermal sublayer, the very high values of Pr_t do not influence the thermal accuracy near the wall. LS has generally higher dimensionless temperature T^+ profiles with the definitions $T^+ = T/T_\tau$ and $T_\tau = q_w/(\rho c_p u_\tau)$ than LB (figure 6). Applying Pr_t as constant results in a too high thermal diffusive calculation and consequently in too low T^+ values. The correlation of Notter results in the highest T^+ profiles. This effect is obvious looking at the profiles of Pr_t. Kays, Cebeci and Lin have nearly the same profile and show the best results in comparison to the exact T^+ and a_t values. Generally, the results show that the validation of Pr_t necessarily includes the turbulence model as well as the numerical solution process. The Notter correlation implies a wrong premise, as described by Churchill [8]. The Lin correlation is similar structured as the Yakhot equation and implicit. Kays carved out that his very simple, explicit correlation gives approximately equivalent results as the Yakhot [7] and so as the Lin correlation. It appears that the models of Kays, Lin and Cebeci yield comparable results and perform better than Notter and Pr_t constant with the most simple complexity by Kays.

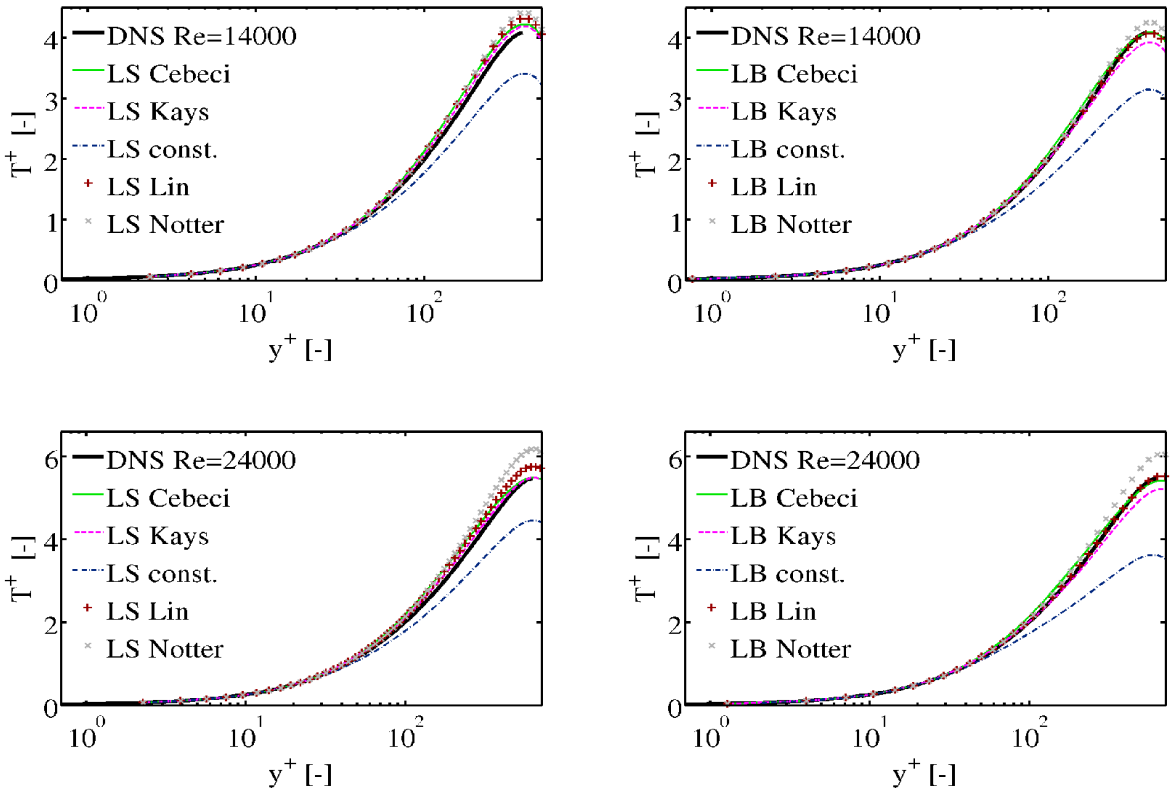

Figure 6: Dimensionless temperature profiles for different correlations of *Prt* with different turbulence models and Reynolds numbers as a function of y^+

In a fully developed channel flow the Boussinesq approach is fulfilled regarding the maximum velocity and the zero crossing of $\overline{u_1' u_2'}$. Linear and nonlinear eddy viscosity models determine all terms of the turbulent shear stress depending on the velocity gradient. These models unify the maximum of the velocity and the zero crossing of the total shear stress at one position. But this assumption cannot be applied to a shear flow in general. Therefore, the next validation case is the concentric annular pipe flow.

3.2 Fully developed concentric annular pipe flow

The turbulent flow of fully developed annular channels as shown in figure 7 has been extensively studied. The experimental works of Rehme [14], Kang et. al. [15], the simulations with DNS by Chung et. al. [10], [16] or general analyzes by Kaneda et. al. [17] can exemplarily be listed.

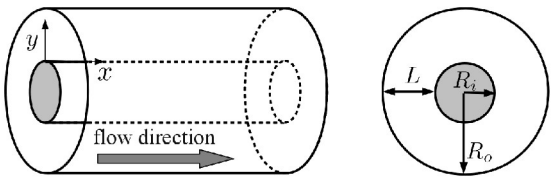

Figure 7: Schematic diagram of the fully developed concentric annular pipe flow

Here, the Reynolds number $Re_{D_h} = \overline{u}_{bulk} D_h / \nu = 4450$ is defined using the hydraulic diameter $D_h = L$. The Boussinesq approach is not fulfilled, analyzing the position of the maximum velocity $y(u_{max}) = 0.320$ in comparison with the zero crossing of the turbulent shear stress $y(\tau_{t,12} = 0) = 0.305$ of the DNS [10]. That flow asymmetry increases with decreasing radius ratio, in this case $R_i / R_o = 0.1$. It is a major issue if linear models only relying on velocity gradients can depict the velocity profile and the turbulence properties as ν_t and the Reynolds stresses R_{ij} adequately.

The RANS simulations with LS determine $y(u_{max}) = y(\tau_{t,12}) = 0.295$. Generally, the validation of LS by DNS shows a good agreement of the velocity profile (figure 8) and of R_{12} (figure 9) near the outer radius. But close to the inner radius, the velocity gradient becomes too low and $|R_{12}|$ is too low, respectively.

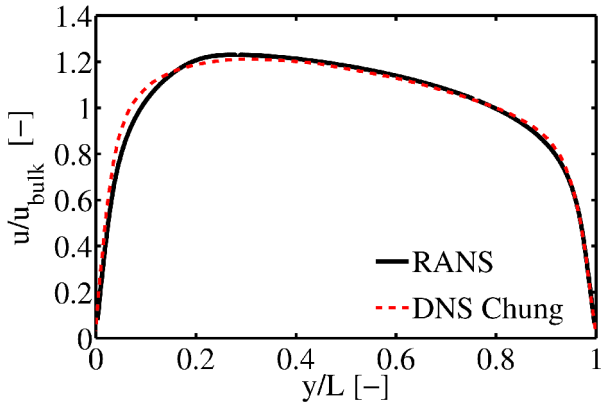

Figure 8: Comparison of the velocity profile of the concentric annular pipe flow over *y/L*

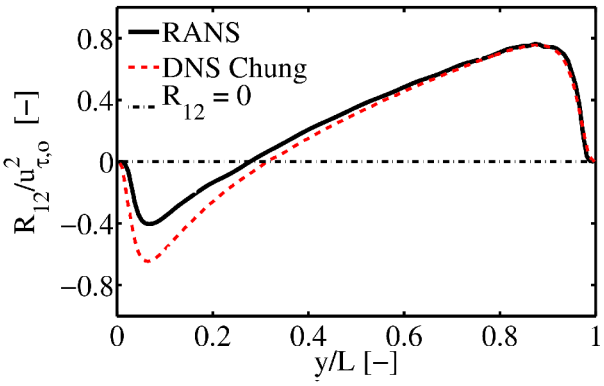

Figure 9: Comparison of the Reynolds stress profile of the concentric annular pipe flow over *y/L*

The inaccurate ν_t near the inner wall, using LS, influences the modeled heat fluxes, and so the correlations of Pr_t must account for this deficits in the near wall region in a adequate manner. Recommendations for a more precise description of Prt correlations with respect for the turbulent heat transfer in liquid metal shear flows may be taken from Grötzbach [1].

3.3 Heated rod in a vertical annulus

Figure 10 displays the experimental setup of a generic experiment conducted in KALLA. Hereby, a rod heated with a constant heat flux q_w is concentrically embedded in a pipe flow.

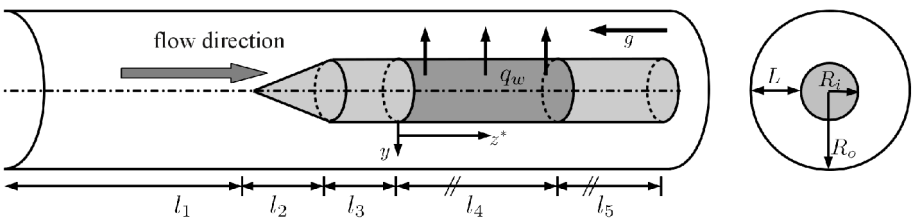

Figure 10: Schematic diagram of the geometric setup of the heated rod simulations

All spacers, the Pitot tube to measure the local velocity and the flow straightener are neglected in the simulations. More details on the experimental set-up may be taken from [11]. Regarding the inlet condition, an isothermal turbulent hydraulically fully developed pipe flow with a radius $R_o = 0.03m$, it is assumed at $l_1 = 0.35m$ upstream the rod, which does not match the experimental findings fully as reported in [18]. The rod dimensions are $R_i = 0.0041m$, $l_2 = 0.0246m$ and $l_3 = 0.028m$. The rod is uniformly heated with $Q = 3kW$ resp. $q_w = Q/(2l_4\pi R_i)$ at position $z^* = 0$ with $z^* = z/(2R_i)$ along $l_4 = 0.86m$. It is followed by an unheated zone, which has been chosen in the numerical simulations to a length $l_6 = 0.34m$. The Reynolds number of the investigated cases are $Re_{D_h} = 237000$ and $Re_{D_h} = 59100$. The thermophysical properties of the fluid relations for ν, α, β and the heat capacity c_p have been applied, according to the correlations from the Liquid metals handbook [19] for LBE, using eqs. (1), (2) and the LS turbulence model including buoyancy.

In figure 11 the development of the velocity profiles for mixed and forced convection, using a constant Pr_t, are shown for different *z**. Due to the heating of the LBE near the rod, the buoyancy influences the velocity profile and the turbulence characteristics. The maximum velocity decreases from *z* = 0* to *z* = 3.55* and increases from *z* = 3.55* to *z* = 7.55*. The position of the maximum moves from *y/L = 0.1* at *z* = 0* to *y/L = 0.16* for both higher z*. In comparison, the case with forced convection reduces continuously its maximum velocity with higher z* values. The position of the maximum velocity rises to higher y/L values. The velocity increment of the mixed convection case near the rod is caused by the buoyancy effects and influences thus the thermal field.

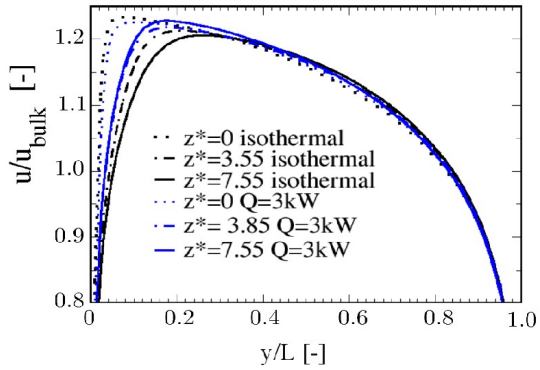

Figure 11: Comparison of the velocity profiles for isothermal and heated boundary conditions with a constant Pr_t as function of *y/L* for *Re = 59100*

Buoyancy has no perceivable effect on the velocity profile for *Re = 237000,* and so this case can be considered as forced convection. In figure 12 the temperature profiles over the gap height for two *z** values are given. The wall near temperature gradient in wall normal direction is for all models correctly given, because the turbulent heat fluxes and the convective heat transfer is negligible. But in the inner part, the faultiness of the velocity profile and ν_t due to the LS model influences the accuracy. Therefore, modeling Pr_t as constant shows the best wall temperature results in comparison to experimental data. Applying the Pr_t correlations even worsens the results. The highest heating occurs with the Cebeci and the Notter correlations, whereas the wall

temperature values by the Kays and Lin correlations show wall temperature values which lie in between.

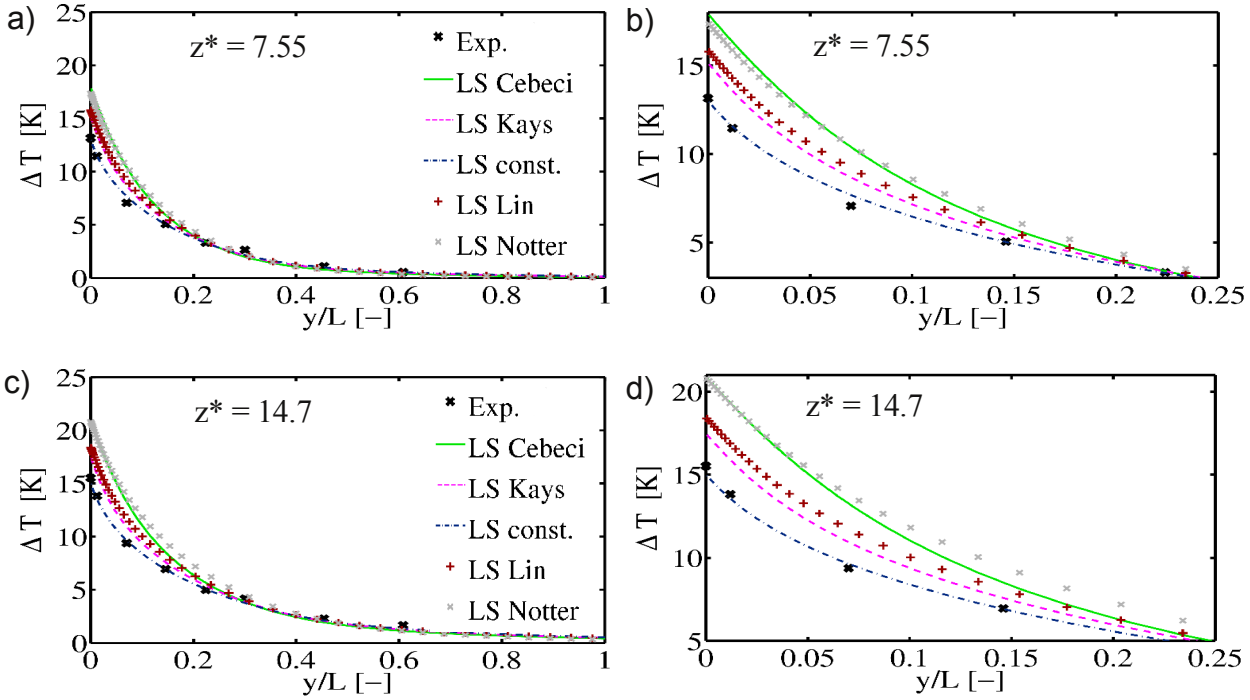

Figure 12: Comparison of the temperature profiles at position *z* = 7.55* a) over *y/L*, b) near the rod and *z* = 14.7* c) over *y/L*, d) near the rod for different Pr_t correlations and experimental data for *Re = 237000*

Figure 13 shows the temperature profiles for the mixed convection case. The extension of the thermal boundary layer, observed in the experiments, is considerably larger than predicted by any simulation even at small z* values. This means that the radial heat transfer is different. It can be effected due to the too less ν_t of LS or by a too less buoyancy turbulence production term in the *k*-equation. Again, the near wall temperature without Pr_t correlation show the best results in comparison to the experimental data. Lin and Kays exhibit the highest temperature values followed by Cebeci and finally Notter. To sum up, LS determines ν_t near the inner wall in a concentric annular pipe flow too low, as described in 3.2. The Pr_t correlations reduce in combination with LS α_t excessively. This results in too high temperature gradients near the inner wall. Hence, a more accurate modeling of ν_t by the turbulence model is required, or the Pr_t correlations have to be adjusted with the flow type to correct its specific modeling faultiness. Algebraic stress models (ASM) with a more accurate determination of the Reynolds stresses like [20] should be used and should be exanded with the Kays, Lin or Cebeci correlation or even with an algebraic heat flux model. But latter, a correct computation of all Reynolds stresses is necessary for an advancement of the thermal field which not all ASM achieve.

4. Conclusion

Reynolds averaged simulations applying Pr_t correlations have been compared with DNS and experimental data of shear flows with low *Pr* mediums. The enhanced turbulent heat flux modeling showed an improved thermal accuracy in comparison to a constant Pr_t in a fully

developed channel flow. The turbulence model influences the thermal characteristics, since the turbulent heat fluxes are connected to the Reynolds stresses.

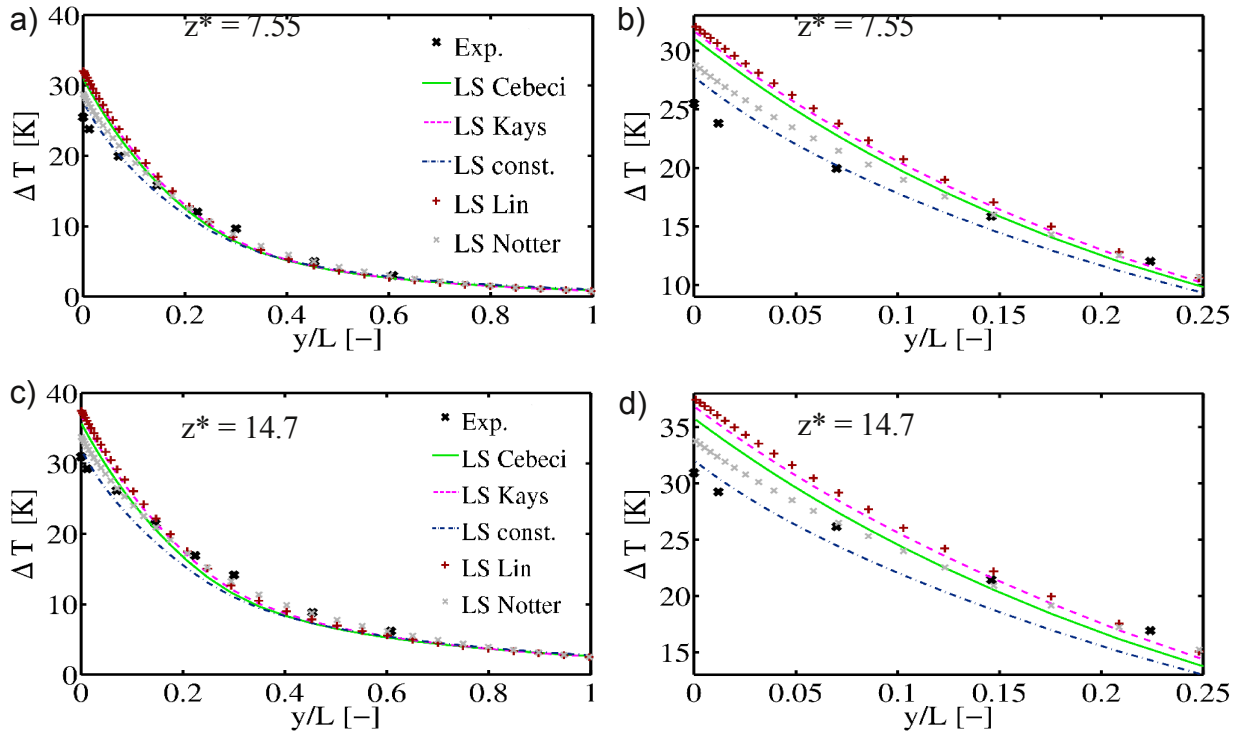

Figure 13: Comparison of the temperature profiles at position *z* = 7.55* a) over *y/L*, b) near the rod and *z* = 14.7* c) over *y/L*, d) near the rod for different Pr_t correlations and experimental data for *Re = 59100*

It appeared the need to adjust the ν_t inaccuracy of the turbulence model by altering the Pr_t correlations for the respective shear flow type and the turbulence model. Exemplary, the validation of the heated rod experiment for forced and mixed convection from KALLA showed a better agreement with the temperature profiles using the Launder and Sharma model and a constant Pr_t in comparison to the enhanced models. This was caused by too low modeled turbulent viscosity near the rod. It exhibited that especially for mixed convective flows the radial heat transport is not sufficient. This could be caused by too less ν_t values due to the turbulence model in concentric annular pipe flows or a too less buoyancy turbulence production term in the *k*-equation. In summery, turbulent heat flux models have to be validated including the turbulence model and the flow case type.

5. References

[1] G. Grötzbach, "Anisotropy and buoyancy in nuclear turbulent heat transfer – critical assessment and needs for modeling", Wissenschaftlicher Bericht FZKA 7363, Forschungszentrum Karlsruhe, pp. 1-54.

[2] S. Wallin and A.V. Johansson, "An explicit algebraic Reynolds stress model for incompressible and compressible flows", Journal of Fluid Mechanics, Vol. 403, 2000, pp. 89-132.

[3] V. C. Patel and W. Rodi and G. Scheuerer, "Turbulence Models for Near-Wall and Low Reynolds Number Flows: A Review", *AIAA Journal*, 1984, pp. 1308-1319.
[4] B.A. Younis and C.G. Speziale and T.T. Clark, "A rational model for the turbulent scalar fluxes", *Proceedings of the Royal Society*, Vol. 461, 2005, pp. 575-594.
[5] T. Cebeci, "A model for eddy conductivity and turbulent Prandtl number", *Journal of Heat Transfer*, Vol. 95, 1973, pp. 227-234.
[6] B. Lin and C.C. Chang and C. Wang, "Renormalization group analysis for thermal turbulent transport", *The American Physical Society Review E,* Vol. 63, 2000, pp. 1-11.
[7] W.M. Kays, "Turbulent Prandtl Number – Where Are We? (The 1992 Max Jakob Memorial Award Lecture)", *Journal of Heat Transfer*, Vol. 116, 1994, pp. 284-295.
[8] S.W. Churchill, "A Reinterpretation of the Turbulent Prandtl Number", *Industrial & Engineering Chemistry Research*, 2002, pp. 6393-6401.
[9] H. Abe and H. Kawamura and Y. Matsuo, "Direct Numerical Simulation of a Fully Developed Turbulent Channel Flow With Respect to the Reynolds Number Dependence", *Journal of Fluids Engineering*, Vol. 123, 2001, pp. 382-393.
[10] S.Y. Chung and G.H. Rhee and H.J. Sung, "Direct numerical simulation of turbulent concentric annular pipe flow Part 1: Flow field", *International Journal of Heat and Fluid Flow*, Vol. 23, 2002, pp. 426-440.
[11] A. Loges and T. Baumann and L. Marocco and T. Wetzel and R. Stieglitz, "Experimental investigation on turbulent heat transfer in liquid metal along a heated rod in a vertical annulus", Toronto, Ontario, Canada, 2011 September 25-29.
[12] L. Carteciano and G. Grötzbach, "Validation of turbulence models for a free hot sodium flow jet with different buoyancy flow regimes using the computer code FLUTAN", FZKA 6600, Forschungszentrum Karlsruhe, 2003.
[13] DNS Database of Wall Turbulence and Heat Transfer, http://murasun.me.noda.tus.ac.jp/turbulence
[14] K. Rehme, "Turbulente Strömung in konzentrischen Ringspalten", Habilitation, Kernforschungszentrum Karlsruhe, KfK 2099, 1975.
[15] S. Kang and B. Patil and J.A. Zarate and R.P. Roy, "Isothermal and heated turbulent upflow in a vertical annular channel – Part I. Experimental measurements", *International Journal of Heat and Mass Transfer*, Vol. 44, 2001, pp. 1171-1184.
[16] S.Y. Chung and H.J. Sung, "Direct numerical simulation of turbulent concentric annular pipe flow Part 2: Heat transfer", International Journal of Heat and Fluid Flow, Vol. 24, 2003, pp. 399-411.
[17] M. Kaneda and B. Yu and H. Ozoe and S.W. Churchill, "The characteristics of turbulent flow and convection in concentric circular annuli. Part I: flow", *International Journal of Heat and Fluid Flow*, Vol. 46, 2003, pp. 5045-5057.
[18] J. Zeininger, "Turbulenter Wärmetransport in flüssigem Blei-Wismut an einem vertikalen Heizstab im Ringspalt", Forschungszentrum Karlsruhe, Dissertation, 2009.
[19] OECD/NEA Nuclear Science Committee, Working Party on Scientific Issues of the Fuel Cycle, , "Handbook on Lead-bismuth Eutectic Alloy and Lead Properties, Materials Compatibility, Thermal-hydraulics and Technologies", 2007, ISBN 978-92-64-99002-9
[20] A. Hellsten, "New Two-Equation Turbulence Model for Aerodynamics Applications", Helsinki University of Technology, Laboratory of Aerodynamics, Dissertation, 2004.